DOI: 10.1111/mice.12670

ORIGINAL ARTICLE

COMPUTER-AIDED CIVIL AND INFRASTRUCTURE ENGINEERING WILEY

A decision-making methodology for risk-informed earthquake early warning

Gemma Cremen[1] | **Carmine Galasso**[1,2]

[1] Department of Civil, Environmental and Geomatic Engineering, University College London, London, UK

[2] Science, Technology and Society, Scuola Universitaria Superiore (IUSS) Pavia, Pavia, Italy

Correspondence
Gemma Cremen, Department of Civil, Environmental and Geomatic Engineering, University College London, London, United Kingdom.
Email: g.cremen@ucl.ac.uk

Funding information
European Union's Horizon 2020 research and innovation programme, Grant/Award Number: 821046

Abstract

To maximize the potential of earthquake early warning (EEW) as a credible tool for seismic resilience promotion, it should be combined with next-generation decision-support tools that use advanced risk-based predictions and account for unavoidable malfunctions of the system (i.e., false alarms) to determine whether or not alerts/mitigation actions should be triggered. This work contributes to the required effort by developing a novel end-user-oriented approach for decision making related to very short-term earthquake risk management. The proposed methodology unifies earthquake-engineering-related performance assessment procedures/metrics (for end-user-focused damage and consequence estimation) with multicriteria decision-making tools (to consider end-user preferences toward different types of risks). It is demonstrated for EEW in a hypothetical school building, to specifically investigate the optimal decisions (i.e., "trigger"/"do not trigger" alerts) for a range of earthquake scenarios with varying parameter uncertainties. In particular, it is found that the best action for a given ground-shaking intensity can depend on stakeholder (end-user) preferences.

1 | INTRODUCTION

Earthquake early warning (EEW) is undergoing a growth in popularity worldwide as an attractive tool for enhancing and promoting seismic resilience in urban areas (e.g., Cauzzi et al., 2016; Gasparini et al., 2011). Specifically, EEW systems rely on real-time data telemetry to provide information about ongoing earthquakes, enabling various stakeholders (end-users) to take effective steps for reducing potential harmful impacts of an event before strong shaking occurs at a target site (e.g., Allen & Melgar, 2019; Hsu et al., 2016; Panakkat & Adeli, 2008; Rafiei & Adeli, 2017; Satriano, Wu et al., 2011). This type of technology is currently operating in nine countries, and is being tested for feasibility in many more (Cremen & Galasso, 2020; Cremen et al., 2021).

To date, innovations in EEW have largely focused on seismological aspects and hazard models. For example, one of the most recent advances in EEW is the use of machine learning to discriminate seismic signals from noise, for more reliable earthquake detection (Meier et al., 2019). However, to maximize the potential of these technologies as effective risk-management tools, there also needs to be a focus on developing and incorporating next-generation decision-support tools. These tools use advanced engineering-based consequence predictions related to the corresponding hazards, so that stakeholders can be informed of appropriate risk mitigation actions to

take when necessary (e.g., Bozza et al., 2017; Ouyang & Fang, 2017; Sharma et al., 2020; Tesfamariam et al., 2010; Zhou et al., 2018).

Some work connected to this requirement has already been done in the literature. For example, Grasso (2005), Iervolino, Giorgio et al. (2007), and Iervolino (2011) introduced a probabilistic loss-driven decision-making framework for EEW. This was advanced in Wu et al. (2013) through the integration of basic decision theory, and the updated methodology was applied to the automated process of elevator control in Wu et al. (2016). Additional examples of EEW risk-based decision-making procedures proposed in the literature are those documented in Grasso et al. (2007), Salzano et al. (2009), Wang et al. (2012), and Le Guenan et al. (2016).

However, most of the aforementioned studies rely on the concept of equally weighted cost–benefit analysis and/or only one loss-related criterion to support decision making. These types of approaches have several disadvantages. First, cost–benefit analyses require the use of questionable assumptions about the dollar value of nonmonetary losses (such as casualties and functional disruption), which may not be accurate and can lack consistency across different jurisdictions (e.g., Krawinkler et al., 2006; Viscusi & Masterman, 2017). Second, these approaches do not (or do not easily) enable different dimensions of risk (e.g., public safety, economic loss, and functionality) to be distinguished in the decision-making process, which is problematic if the stakeholder does not place equal importance on each risk type (May, 2004). Third, they do not account for risk tolerance, which is an important consideration for engineering-related applications (Stewart & Melchers, 1997). While the work of Wu et al. (2013) leverages expected utility theory in an attempt to overcome this final limitation, the basis of their decision-making procedure remains a cost–benefit analysis. As a further improvement, Le Guenan et al. (2016) use multiattribute utility theory applied to various risk-tolerance scenarios, which theoretically eliminates all of the above restrictions. But the proposed methodology only works for binary action cases (e.g., "trigger" or "do not trigger" an EEW alarm), uses a simplistic time-independent description of real-time seismic hazard, and relies on a deterministic engineering-agnostic damage-to-loss relationship, which make it unsuitable for a broad range of short-term seismic risk management purposes.

This paper proposes an advanced methodology that overcomes all of the previously identified shortcomings in two main ways. First, it implements a general multicriteria decision-making (MCDM) approach, which enables multiple mitigation actions to be evaluated for various dimensions of uncertain risk. The particular MCDM technique discussed in the paper has been successfully implemented in previous work to determine optimal seismic retrofitting options (Caterino et al., 2008, 2009; Gentile & Galasso, in press) and more general emergency response solutions (Zhang et al., 2016), for example. Second, MCDM is coupled with a modified version of the performance-based earthquake engineering (PBEE) framework (Moehle & Deierlein, 2004) that incorporates evolutionary Bayesian real-time seismic hazard analysis. This framework forms a convenient mathematical foundation for real-time probabilistic seismic risk decision making that (1) accounts for all important sources of uncertainty associated with EEW and (2) considers multiple consequence variables. Furthermore, traditional PBEE has been used to choose optimal actions in many other earthquake-engineering-related applications, such as seismic design (Goda & Hong, 2006), seismic retrofitting (Porter et al., 2006), seismic sensor implementation (Cremen & Baker, 2018), postearthquake repair scheduling (Xiong et al., 2020), and parametric earthquake insurance (Goda, 2015), as well as MCDM problems involving household recovery (Burton et al., 2018) and design optimization (Mosalam et al., 2018; Saadat et al., 2014).

This paper is organized in the following manner. The proposed methodology is developed within Section 2, which specifically details how MCDM and PBEE are uniquely unified in the context of risk-driven EEW. Section 3 involves an application of the methodology to EEW in a hypothetical school, and the optimal decision is investigated for various levels of information on the incoming earthquake. Finally, discussion and conclusions on the study are provided in Section 4.

2 | METHODOLOGY

The proposed methodology consists of a number of well-defined, computer-implementable steps (i.e., algorithm). It evaluates a group of end-user selected EEW mitigation actions ($\{A_i\}$), as well as the option of taking no action ($\overline{A}$), based on case-specific values associated with a set of corresponding uncertain consequence criteria ($\{C_j\}$) that are assigned weights ($\{w_j\}$) to reflect their importance in line with end-user preferences. The explicit incorporation of these preferences and the fact that the criteria do not need to be given a monetary value both represent improvements over conventional dollar-based (cost–benefit) decision-making procedures used in past EEW studies, as discussed in the previous section. The methodology is comprised of three main steps. The first step represents the real-time PBEE module of the algorithm (Mod_PBEE), which computes the probabilistic consequences ($\{C_j\}$) for each action and uses an evolutionary seismic hazard analysis to facilitate the integration with existing seismological

TABLE 1 Explanation of consequence matrix inputs for Step 1 of the proposed methodology

	C_1 Casualties (Number)	C_2 Downtime (days)	C_3 Direct cost ($)
A_1	Expected casualties from possible false alarm + expected casualties from estimated shaking that is not eliminated with mitigation action 1, $[E^{A_1}(C_1^{A_1}\|\mathbf{d})]$	Expected disruption from possible false alarm + expected downtime from estimated shaking that is not eliminated with mitigation action 1, $[E^{A_1}(C_2^{A_1}\|\mathbf{d})]$	Expected reconditioning cost from possible false alarm + expected repair cost from estimated shaking that is not eliminated with mitigation action 1, $[E^{A_1}(C_3^{A_1}\|\mathbf{d})]$
⋮	⋮	⋮	⋮
⋮	⋮	⋮	⋮
⋮	⋮	⋮	⋮
A_{N_a}	Expected casualties from possible false alarm + expected casualties from estimated shaking that is not eliminated with mitigation action N_a, $[E^{A_{N_a}}(C_1^{A_{N_a}}\|\mathbf{d})]$	Expected disruption from possible false alarm + expected downtime from estimated shaking that is not eliminated with mitigation action N_a, $[E^{A_{N_a}}(C_2^{A_{N_a}}\|\mathbf{d})]$	Expected reconditioning cost from possible false alarm + expected repair cost from estimated shaking that is not eliminated with mitigation action N_a, $[E^{A_{N_a}}(C_3^{A_{N_a}}\|\mathbf{d})]$
$\overline{A}$ (no action)	Expected casualties from estimated shaking, $[E^{\overline{A}}(C_1^{\overline{A}}\|\mathbf{d})]$	Expected downtime from estimated shaking, $[E^{\overline{A}}(C_2^{\overline{A}}\|\mathbf{d})]$	Expected repair cost from estimated shaking, $[E^{\overline{A}}(C_3^{\overline{A}}\|\mathbf{d})]$

algorithms for EEW. The second step integrates the outputs of Mod_PBEE within the MCDM module (Mod_MCDM), which accounts for the criteria-specific risk priorities of stakeholders ($\{w_j\}$). The results of Mod_MCDM are used to select the optimal decision in the final step of the methodology (Mod_Decision).

Step 1: Develop a consequence matrix (Mod_PBEE). For all N_a identified actions and $\overline{A}$, the values associated with each of the N_c consequence criteria are first assembled in a consequence matrix (see Table 1—note that the criteria shown are merely representative and do not constitute an exhaustive list). The value of the jth criterion for $\overline{A}$ is equivalent to the expected value of the consequence $E^{\overline{A}}(C_j^{\overline{A}}|\mathbf{d})$ for the incoming ground shaking. $E^{\overline{A}}(C_j^{\overline{A}}|\mathbf{d})$ is estimated using PBEE theory and physical measurements from a network of seismic stations ($\mathbf{d}$), according to the performance-based earthquake early warning (PBEEW) framework developed by Grasso (2005) and Iervolino, Giorgio et al. (2007):

$$E^{\overline{A}}(C_j^{\overline{A}}|\mathbf{d}) = \int_{c_j^{\overline{A}}} \int_{\mathbf{dm}} \int_{\mathbf{im}} c_j^{\overline{A}} f^{\overline{A}}\left(c_j^{\overline{A}}|\mathbf{dm}\right) f(\mathbf{dm}|\mathbf{im}) \, f(\mathbf{im}|\mathbf{d}) \, dc_j^{\overline{A}} \, d\mathbf{dm} \, d\mathbf{im} \tag{1}$$

$f(a|b)$ is the probability density function (pdf) of a conditional on b, $\mathbf{dm}$ is a scalar or vector measure of damage level, and $\mathbf{im}$ is a vector of ground shaking intensities. $f(\mathbf{dm}|\mathbf{im})$ can be obtained using a building-level fragility function (scalar damage) or through an intermediate engineering demand/structural response parameter (EDP) variable for component-level performance assessment procedures (vector damage); in the latter case, $f(\mathbf{dm}|\mathbf{im}) = \int_{\mathbf{EDP}} f(\mathbf{dm}|\mathbf{edp}) f(\mathbf{edp}|\mathbf{im}) \, d\,\mathbf{EDP}$.

$f(\mathbf{im}|\mathbf{d})$ is the pdf of $\mathbf{im}$ given current knowledge on the incoming event. $\mathbf{d}$ could comprise the vectors of information used by the implemented seismological EEW algorithm—for example, ElarmS (Brown et al., 2011) or PRESTo (Satriano, Elia et al., 2011)—to estimate magnitude and location in real time. If the applicable seismological algorithm provides point estimates of the magnitude ($\hat{m}$) and location of the incoming event, then $\mathbf{d} = \{\hat{m}, \hat{r}\}$ (where $\hat{r}$ is the corresponding estimate of the distance from the source to a target site of interest) and:

$$f(\mathbf{im}|\mathbf{d}) = f(\mathbf{im}|\{\hat{m}, \hat{r}\}) \tag{2}$$

can be computed with the aid of a ground motion model (GMM), for example. Where the seismological algorithm uses the seismic network measurements to estimate the incoming ground shaking at a site ($\hat{\mathbf{im}}$), $\mathbf{d} = \hat{\mathbf{im}}$ and $E^{\overline{A}}(C_j^{\overline{A}}|\mathbf{d})$ is found using the following simplified version of Equation (1):

$$E^{\overline{A}}\left(C_j^{\overline{A}}|\mathbf{d}\right) = E^{\overline{A}}\left(C_j^{\overline{A}}|\hat{\mathbf{im}}\right) = \int_{c_j^{\overline{A}}} \int_{\mathbf{dm}} c_j^{\overline{A}} f^{\overline{A}}\left(c_j^{\overline{A}}|\mathbf{dm}\right) f(\mathbf{dm}|\hat{\mathbf{im}}) \, dc_j^{\overline{A}} \, d\mathbf{dm} \tag{3}$$

It can be seen from Table 1 that the expected value of the jth criterion for the ith action, $E^{A_i}(C_j^{A_i}|\mathbf{d})$ includes (1) the consequence associated with a potential false alarm, $E(C_{ij}^{FA}|\mathbf{d})$, as well as (2) the action-, criterion-, and

TABLE 2 Sample decision matrix developed in Step 2 of the proposed methodology

	C_1 Casualties (Number)	C_2 Downtime (days)	C_3 Direct cost ($)
A_1	$r_{A_1,C_1}w_1$	$r_{A_1,C_2}w_2$	$r_{A_1,C_3}w_3$
⋮	⋮	⋮	⋮
⋮	⋮	⋮	⋮
⋮	⋮	⋮	⋮
A_{N_a}	$r_{A_{N_a},C_1}w_1$	$r_{A_{N_a},C_2}w_2$	$r_{A_{N_a},C_3}w_3$
$\overline{A}$ (no action)	$r_{\overline{A},C_1}w_1$	$r_{\overline{A},C_2}w_2$	$r_{\overline{A},C_3}w_3$

event-specific proportion of the corresponding PBEE-based consequence for $\overline{A}$ that cannot be mitigated, $E^{\overline{A}}(C_j^{\overline{A}}|\mathbf{d})\alpha_{ij}(\mathbf{d})$ (where $\alpha_{ij}(\mathbf{d})$ is a scalar value between 0 and 1). False alarms occur when a risk-mitigation action turns out to be unnecessary for the level of shaking actually observed, that is, when no vulnerable component in the building (either structural or nonstructural) is damaged. The probability of a false alarm, ($p(FA|\mathbf{d})$) may be calculated as follows:

$$p(FA|\mathbf{d}) = (1 - p(Cp|\mathbf{d}))\left(1 - \int_{\mathbf{dm}} f(\mathbf{dm}|\{\mathbf{d}, \overline{Cp}\})\, d\mathbf{dm}\right) \tag{4}$$

where Cp is the occurrence of collapse and $\overline{Cp}$ is its complementary. $E(C_{ij}^{FA}|\boldsymbol{d})$ is then computed using the following equation:

$$E\left(C_{ij}^{FA}|\mathbf{d}\right) = c_{ij}^{FA}\, p\,(FA|\mathbf{d}) \tag{5}$$

where c_{ij}^{FA} is the expected consequence due to false alarm disruption for the jth criterion and the ith action. Both c_{ij}^{FA} and $\alpha_{ij}(\mathbf{d})$ are obtained from stakeholder feedback.

Examples of potential EEW actions for a building include: A_1: "duck, cover, and hold" (DCHO) and A_2: "evacuate the building." A_1 will likely lead to larger expected casualties for an incoming event than A_2, since DCHO will not protect occupants if the building collapses. However, A_2 requires a disruptive (and potentially costly) period of building reoccupation in the event of a false alarm, which is avoided for A_1. Potential EEW actions for a bridge include: A_1: "shut the bridge" and, based on the work of Maddaloni et al. (2011), A_2: "keep the bridge open, using semi-active control strategies to optimize its real-time structural response." Here, A_1 will result in lower shaking-related—but higher false-alarm-related—consequences than A_2, overall. The correct action to take for any structural type will depend on stakeholder preferences toward specific types of consequences, which are accounted for in Step 2 of the algorithm.

Step 2: Develop a decision matrix (Mod_MCDM). The consequence matrix values from Mod_PBEE are first normalized as follows:

$$r_{A_i,C_j} = \frac{E^{A_i}\left(C_j^{A_i}|\mathbf{d}\right)}{\sqrt{\sum_{k=1}^{N_a}\left(E^{A_k}\left(C_j^{A_k}|\mathbf{d}\right)\right)^2 + \left(E^{\bar{A}}\left(C_j^{\bar{A}}|\mathbf{d}\right)\right)^2}}, \tag{6}$$

where r_{A_i,C_j} is the normalized value of the jth criterion for the ith action, and all other variables are as defined for Mod_PBEE. r_{A_i,C_j} values are then weighted according to stakeholder preferences (priorities) toward each criterion, to form the decision matrix (Table 2).

The corresponding weights ($\{w_j\}$) may be obtained using the analytic hierarchy process (Saaty, 1980) for example. This procedure involves the stakeholder performing a series of pairwise comparisons for each criterion, based on qualitative phrasing for relative importance that is quantified (for analysis purposes) on a scale from 1/9 to 9. One on the quantitative scale implies that the stakeholder considers both criteria to be equally significant, 5 indicates that the stakeholder believes criterion X is strongly important over criterion Y, 9 means that criterion X has extreme importance to the stakeholder compared to criterion Y, all other values between 1 and 9 signify intermediate judgments to those stated, and reciprocal values indicate equivalent opinions of criterion Y compared to criterion X. The quantitative results of the comparison are summarized in an $N_c \times N_c$ matrix, the principal right eigenvector of which is equivalent to $\{w_j\}$.

Step 3: Identify the optimal decision (Mod_Decision). The final part of the methodology determines the optimal decision among $\{A_i\}$ and $\overline{A}$. This first involves quantifying the best and worst values for each criterion across all possible options. Since the criteria in this case are negative consequences, the best value of the jth criterion (v_j^+) is its minimum value, that is, $v_j^+ = \min_j(r_{A_1,C_j}w_j, \ldots, r_{A_{N_a},C_j}w_j, r_{\overline{A},C_j}w_j)$ and the worst value (v_j^-) is its maximum, that is, $v_j^- = \max_j(r_{A_1,C_j}w_j, \ldots, r_{A_{N_a},C_j}w_j, r_{\overline{A},C_j}w_j)$. The total distance of a given action A_i from the best (y_i^+) and worst (y_i^-) solutions are then, respectively, calculated as

follows:

$$y_i^+ = \sqrt{\sum_{j=1}^{N_c} \left(v_j^+ - (r_{A_i,C_j} w_j) \right)^2}, \tag{7}$$

$$y_i^- = \sqrt{\sum_{j=1}^{N_c} \left(v_j^- - (r_{A_i,C_j} w_j) \right)^2} \tag{8}$$

The optimal action is the one with the largest S_i value, calculated according to:

$$S_i = \frac{y_i^-}{y_i^+ + y_i^-} \tag{9}$$

Note that the final two steps have specifically been described in terms of the TOPSIS (*Technique for Order Preference by Similarity to Ideal Solution*) approach (Caterino et al., 2009; Yoon & Hwang, 1995), which is adopted in the case-study application (Section 3). However, the risk attitudes of stakeholders could additionally be explicitly accounted for by alternatively using multiattribute utility theory (Dyer, 2005), without changing the overall structure of the system. In that case, the r_{A_i,C_j} values of the decision matrix in Step 2 would be replaced with normalized utility values (u_{A_i,C_j}) that depend on the values of the consequence matrix and the risk tolerance of stakeholders. $u_{A_i,C_j} w_j$ would then be aggregated across each option (either additively or multiplicatively), and the optimal decision would be the one that maximizes the final value.

The developed algorithm is provided in Appendix A. This algorithm could be packaged as a state-of-the-art risk-driven plug-in to existing EEW platforms, providing operational EEW with high-resolution structure-specific decision-making capabilities for the first time. The computational assimilation of the plug-ins and the seismology-focused algorithms of the current platforms would be facilitated by the PBEEW architecture, outlined in Equation (1).

3 | EXAMPLE APPLICATION TO A SCHOOL BUILDING

The proposed methodology is now demonstrated, using a hypothetical school located in Palo Alto, California (37.4° North and 122.15° West). The choice of location is timely, given that California is beginning to benefit from public alerts issued by the ShakeAlert EEW system (e.g., McBride et al., 2020). This system combines point-source and finite-source algorithms, to create an alert for incoming earthquakes with estimated magnitudes of at least 4.5 (e.g., Chung et al., 2020). A hypothetical school is chosen for the following reasons: (1) The examined consequence weighting scenarios may not accurately reflect the priorities of actual decision makers in a real school, posing an ethical challenge; (2) It enables the general applicability of the method to be emphasized, demonstrating that it is not just limited to one particular building or even one specific structural/occupancy type; and (3) The ShakeAlert EEW system does not (yet) facilitate building-specific public EEW alarms, making it impossible to apply the methodology to a real Californian building equipped with EEW.

While it is possible to consider multiple actions using the proposed methodology (as discussed in Sections 1 and 2), it is assumed that there are only two potential risk-management options for this particular case study: "Trigger the EEW alarm" (A_1) and "Don't trigger the EEW alarm" ($\overline{A}$). The target structure of interest is assumed to be a two-story reinforced concrete moment-resisting frame with column-beam connections, in line with typical characteristics of suburban U.S. schools (FEMA, 2010; The National Institute of Building Sciences, 2010). The plan layout of the two-story precast concrete frame school detailed in O'Reilly et al. (2018) is adopted, assuming 4 m (13 feet) floor heights. Additional details on the building model are provided in Appendix C.

Casualties, downtime, and direct cost are selected as the consequence criteria, which are the traditional performance metrics considered in PBEE (Moehle & Deierlein, 2004). $E^{\overline{A}}(C_j^{\overline{A}}|\mathbf{d})$ values are obtained using the component-level FEMA P-58 seismic performance assessment procedure for individual buildings (FEMA, 2018). The FEMA P-58 simplified structural analysis procedure is used, which determines engineering demand as a function of peak ground acceleration (PGA) and spectral acceleration at the building's fundamental period ($Sa(T_1)$), that is, $\mathbf{im} = \{PGA, Sa(T_1)\}$ in Equation (1). Additional information on the inputs to FEMA P-58, including the structural and nonstructural components modeled, are provided in Appendix C.

It is assumed that a false alarm does not cause any casualties, results in disruption equivalent to 5% of a day (i.e., 1.2 h—to reorganize classes and ease panicked students), and costs $200 for a structural engineering inspection to verify that no damage has occurred. It is assumed that an alarm eliminates any casualties and laptop (i.e., component "UD" in Appendix C) breakages that are not caused by the building collapsing. A general event-independent consequence matrix for the case study is presented in Table 3.

To reflect a diverse range of potential stakeholder priorities toward the different consequence criteria, the following sets of $\{w_j\}$ values in Table 2 are examined: (1)

TABLE 3 Consequence matrix for the case study EEW application, expressed as a function of generic event parameters, $\mathbf{d}$. $\alpha_{11}(\mathbf{d})$ accounts for collapse casualties. Both $\alpha_{12}(\mathbf{d})$ and $\alpha_{13}(\mathbf{d})$ account for collapse laptop breakages (i.e., failure of component "UD" in Appendix C). $c_{12}^{FA} = 0.05$ and $c_{13}^{FA} = 200$ in line with the false alarm assumptions outlined in Section 3

	C_1 Casualties (Number)	C_2 Downtime (days)	C_3 Direct cost ($)
A_1 = Trigger alarm	$E^{A}(C_1^{A}\|\mathbf{d})\alpha_{11}(\mathbf{d})$	$0.05p(FA\|\mathbf{d}) + E^{A}(C_2^{A}\|\mathbf{d})\alpha_{12}(\mathbf{d})$	$200p(FA\|\mathbf{d}) + E^{A}(C_3^{A}\|\mathbf{d})\alpha_{13}(\mathbf{d})$
$\overline{A}$ = Don't trigger alarm	$E^{\overline{A}}(C_1^{\overline{A}}\|\mathbf{d})$	$E^{\overline{A}}(C_2^{\overline{A}}\|\mathbf{d})$	$E^{\overline{A}}(C_3^{\overline{A}}\|\mathbf{d})$

$w_1 = w_2 = w_3 = 0.333$ (i.e., a stakeholder has equal preference for all criteria); (2) $w_1 = 0.5$ and $w_2 = w_3 = 0.25$ (i.e., a stakeholder has higher preference for mitigating casualties); (3) $w_2 = 0.5$ and $w_1 = w_3 = 0.25$ (i.e., a stakeholder has higher preference for mitigating downtime); and (4) $w_3 = 0.5$ and $w_1 = w_2 = 0.25$ (i.e., a stakeholder has higher preference for mitigating direct costs). Sections 3.1–3.3 investigate the optimal EEW triggering decision, using three different types of information for estimating $E^{\overline{A}}(C_j^{\overline{A}}|\mathbf{d})$.

Note that the proposed approach is not compared with previous EEW decision-making methodologies discussed in Section 1, since this would require: (1) tenuous assumptions about the dollar value of downtime and casualties or (2) simplified building-level fragility models and deterministic damage-to-loss relationships, which are not compatible with the advanced PBEE approach of our study. In both cases, discrepancies in the final results would arise due to the loss or damage assumptions required as well as because of the different decision-making approaches adopted, leading to unfair comparisons.

3.1 | Optimal decision as a function of ground shaking

The optimal decision is first examined for a given level of ground shaking, to determine how often the EEW alarm is triggered. This analysis is mathematically equivalent to a case in which the seismological algorithm accurately estimates the shaking intensity at the site. Therefore, this examination uses $E^{\overline{A}}(C_j^{\overline{A}}|\mathbf{d})$ values computed according to Equation (3), for $\hat{\mathbf{im}} = \mathbf{im}$. 2018 US National Seismic Hazard Model (Petersen et al., 2020) site-specific hazard curves are used (for site class D, in line with the soil properties discussed in Section 3.2). A uniform hazard approach is adopted to determine the frequency at which the examined shaking levels (i.e., $Sa(T_1) \leq 0.3g$) are exceeded.

Figure 1 displays the results of this analysis. As expected, the optimal decision for small shaking intensities is $\overline{A}$ due to the low potential for damage at these levels and therefore the high probability of a false alarm. The intensity at which using the alarm becomes the optimal decision depends on stakeholder preferences. It is triggered as low as $Sa(T_1) = 0.12g$ (or approximately once every 10 years on average) when casualties are prioritized, which is partly explained by the assumption of no casualty consequences for a false alarm. However, it is only triggered for $Sa(T_1)$ values in excess of $0.22g$ (i.e., approximately once every 20 years on average) when downtime is treated as the most important risk criterion. Variation in the optimal decision for different criteria weighting is a notable finding, which confirms the importance of accounting for stakeholder preferences when designing a decision-support tool for earthquake risk management.

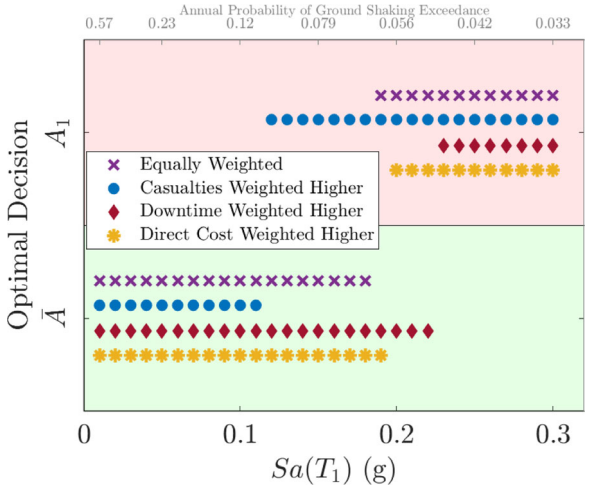

FIGURE 1 Identifying the optimal EEW decision in terms of ground shaking intensity (represented as spectral acceleration at the building's fundamental period). Note that A_1 is the action of triggering the EEW alarm and $\overline{A}$ means that no action is taken

3.2 | Optimal decision as a function of magnitude and distance estimates

Optimal actions for incoming earthquakes are now investigated, assuming that the seismological algorithm provides accurate estimates of magnitude and epicentral location. Thus, $E^{\overline{A}}(C_j^{\overline{A}}|\mathbf{d})$ values are computed using Equations (1) and (2), for $\{\hat{m}, \hat{r}\} = \{m, r\}$ (where r is the true epicentral distance value).

Given the focus on scenario events in this case, $f(\mathbf{im}|\{m, r\})$ is computed according to the conditional mean spectrum approach proposed by Baker and Cornell (2005, 2006). $f(Sa(T_1)|\{m, r\})$ is first determined using the

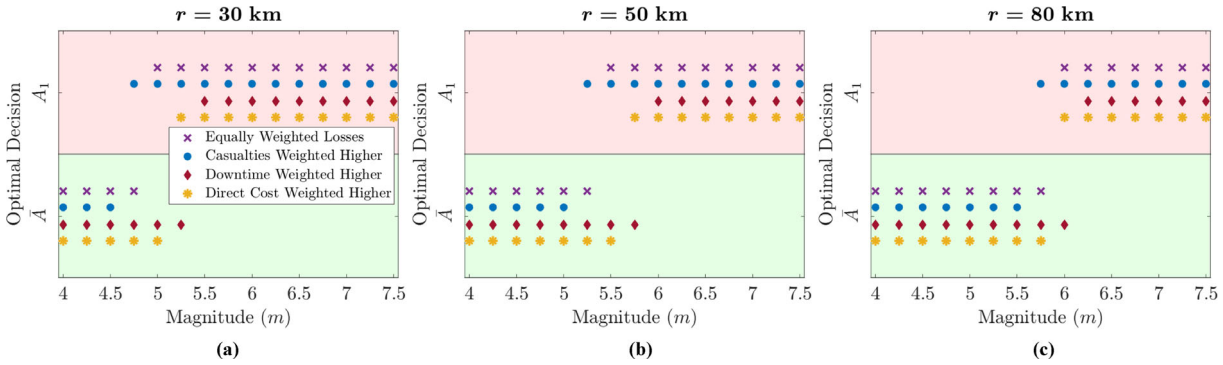

FIGURE 2 Identifying the optimal EEW decision in terms of magnitude, for three epicentral distances: (a) $r = 30$ km, (b) $r = 50$ km, and (c) $r = 80$ km. Note that A_1 is the action of triggering the EEW alarm and $\overline{A}$ means that no action is taken

GMM proposed by Boore et al. (2014) for Western U.S. shallow crustal seismicity and assuming strike-slip faulting to reflect the style of the seven most prominent Bay Area faults. This model requires a rupture distance measure (r_{JB}) as input. r is converted to r_{JB} using adjustment factors provided in Thompson and Worden (2018) for strike-slip faulting in active crustal regions. Uncertainty in the conversion is accounted for by amplifying the standard deviation of the GMM as suggested by the authors. The shear-wave velocity input of the GMM (i.e., $Vs30$) is set equal to 352.1 m/s, which is the value recorded closest to the chosen site in the compilation of $Vs30$ measurements prepared by Yong et al. (2015). The correlation model of Baker and Jayaram (2008) is then used to find the conditional distribution of PGA, that is, $f(PGA|Sa(T_1), \{m, r\})$, according to eqs. 13 and 14 of Baker and Cornell (2005).

Figure 2 displays the results of this case, for three different values of r: (a) $r = 30$ km; (b) $r = 50$ km; and (c) $r = 80$ km. It is clear that the optimal decision in terms of magnitude and distance is also dependent on stakeholder preferences, underlining the significance of the MCDM component in the proposed methodology. Second, it can be seen that the correct action for a given magnitude and set of stakeholder preferences may change from A_1 to $\overline{A}$ at farther distances, reflecting the larger amplitudes of nearer-source shaking intensities. This observation highlights the importance of accounting for both magnitude and location in EEW algorithms, to avoid potentially costly false alarms; note that some currently operational EEW systems lack this feature, for example, the SASMEX magnitude-triggered seismic alert system in Mexico (Cuéllar et al., 2017). Similarly, the optimal decision for a given distance and set of stakeholder preferences varies as a function of magnitude; an alarm should be triggered for magnitudes near 5 at $r = 30$ km, it should be triggered for magnitudes around 5.5 at $r = 50$ km, and it should be triggered for magnitudes close to 6 at $r = 80$ km.

3.3 | Optimal decision as a function of EEW parameters

The ElarmS EEW algorithm (Brown et al., 2011) is adopted for this example, which is part of the point-source code used in the ShakeAlert system. It is therefore assumed that $\mathbf{d}$ consists of the peak displacements measured during the first 4 s of the P-wave recorded at each station (P_{d_k}), which introduces uncertainty in the magnitude prediction of the EEW system (note that distance uncertainty is neglected, since it is negligible with respect to that of magnitude and ground shaking; Iervolino et al., 2009). In this case, Equation (1) simplifies to:

$$E^{\overline{A}}\left(C_j^{\overline{A}}|\mathbf{d}\right) = \int_M E^{\overline{A}}\left(C_j^{\overline{A}}|\{m,r\}\right) f(m|\mathbf{d})\, dM \tag{10}$$

where the value of $E^{\overline{A}}\left(C_j^{\overline{A}}|\{m,r\}\right)$ is taken directly from the analyses of Section 3.2. $f(m|\mathbf{d})$ is assumed to follow the Bayesian mathematical formulation for real-time magnitude estimation proposed by Iervolino, Galasso et al. (2007). Thus, for N_s peak displacement measurements:

$$f(m|\mathbf{d}) = f(m|P_{d_1}, P_{d_2}, \dots, P_{d_{N_s}}) = \frac{f(P_{d_1}, P_{d_2}, \dots, P_{d_{N_s}}|m) f(m)}{\int_{M_{min}}^{M_{max}} f(P_{d_1}, P_{d_2}, \dots, P_{d_{N_s}}|m) f(m)\, dm} \tag{11}$$

where $f(P_{d_1}, P_{d_2}, \dots, P_{d_{N_s}}|m)$ is the joint conditional pdf of the measurements (i.e., the likelihood function) and $f(m)$ is the prior pdf of the magnitude.

$f(m)$ is based on the Gutenberg–Richter relationship, that is:

$$f(m) = \frac{\beta e^{-\beta m}}{e^{-\beta M_{min}} - e^{-\beta M_{max}}} \tag{12}$$

where M_{min} and M_{max} are, respectively, the minimum and maximum magnitudes considered, $\beta = b/\log_{10}(e)$, and b is the slope of the Gutenberg–Richter magnitude–frequency relation. M_{min} is set as 4. $M_{max} = 7.5$, which is approximately equal to the modal maximum magnitude for Western United States shallow crustal seismicity implemented in Petersen et al. (2014). $b = 0.8$, that is, the relevant regional value used in Petersen et al. (2020). In line with Iervolino, Galasso et al. (2007), it is assumed that the station measurements are independent and identically distributed lognormal random variables, such that the conditional pdf of the peak displacement measured at the kth station may be expressed as:

$$f(P_{d_k}|m) = \frac{1}{\sqrt{2\pi}\sigma_{\ln(P_d)}P_{d_k}} e^{-\frac{1}{2}\left(\frac{\ln(P_{d_k})-\mu_{\ln(P_{d_k})}}{\sigma_{\ln(P_d)}}\right)^2} \quad (13)$$

and the likelihood function for measurements across N_s stations is

$$f(P_{d_1}, P_{d_2}, \ldots, P_{d_{N_s}}|m) = \prod_{k=1}^{N_s} f(P_{d_k}|m) \quad (14)$$

The parameters of the lognormal distribution are provided by the work of Wurman et al. (2007), which determines the magnitude–scaling relationship of the ElarmS algorithm for Northern California. Therefore:

$$\mu_{\ln\left(P_{d_k}\right)} = \frac{1}{1.04\log_{10}(e)}\left[m - 1.27\log_{10}(r_k) - 5.16\right] \quad (15)$$

where r_k is the epicentral distance to the kth station, and

$$\sigma_{\ln P_d} = \frac{0.3}{\log_{10}(e)} \quad (16)$$

based on a visual inspection of the data shown in Figure 3a of the aforementioned paper.

Using Equations (11)–(15), it can be shown that (see Appendix B for full details):

$$f(m|\mathbf{d}) = \frac{e^{\frac{x(\mathbf{d})}{2\sigma^2_{\ln(P_d)}}} e^{-\beta m}}{\int_{M_{min}}^{M_{max}} e^{\frac{x(\mathbf{d})}{2\sigma^2_{\ln(P_d)}}} e^{-\beta m}\, dm} \quad (17)$$

for

$$x(\mathbf{d}) = x_1 m[2d_1 - N_s x_1 m + 2x_1(x_2 d_2 + N_s x_3)] \quad (18)$$

where $x_1 = \frac{1}{1.04\log_{10}(e)}$, $x_2 = 1.27$, $x_3 = 5.16$, $d_1 = \sum_{k=1}^{N_s}\ln(P_{d_k})$, $d_2 = \sum_{k=1}^{N_s}\log_{10}(r_k)$, and all other variables are as defined previously. The convenience of this formulation is noteworthy; d_1 and d_2 (and therefore $E^{\overline{A}}(C_j^{\overline{A}}|\mathbf{d})$) can be precomputed offline for all possible values of P_{d_k}, r_k, and N_s, to facilitate efficient real-time decision making.

The accuracy of the optimal decision predicted as a function of P_{d_k}, r_k, and N_s is now investigated, for simulated events at the location of the 1989 Loma Prieta temblor (37.04° North and 121.88° West), across three case-study sites for the hypothetical school (see Figure 3): (1) the aforementioned site in Palo Alto (PA); (2) a site in San Francisco (SF); and (3) a site in San Jose (SJ). To calculate $E^{\overline{A}}(C_j^{\overline{A}}|\mathbf{im})$, $Vs30$ is assumed to be 224.7 m/s for SF and 234 m/s for SJ, which are the closest measurements recorded by Yong et al. (2015).

The following scenario earthquakes are specifically examined: (1) $m = 5.5$; (2) $m = 6$; and (3) $m = 6.9$ (i.e., the magnitude of the real Loma Prieta event). For each of these events, Equation (13) is used to simulate 2000 P_{d_k} values at a given seismic station, and therefore 2000 values of d_1. Using broadband and strong-motion instrument locations of the Northern California Seismic Network (NCEDC, 2014), the optimal decision is determined when all seismic stations within (a) 10 km; (b) 20 km; (c) 30 km; and (d) 50 km of the earthquake have triggered (Figure 3), which, respectively, corresponds to (a) 4; (b) 13; (c) 29; and (d) 81 triggered stations.

Figure 4 contains summary results of these analyses for PA, SF, and SJ (i.e., the average proportion of the four weighting cases investigated for which a correct decision is obtained, across the 2000 magnitude-dependent sets of simulated EEW parameters), as a function of the simulated magnitudes. Before interpreting the findings, the lead (warning) time available for the different triggered station cases is additionally considered, which is approximated at a given site according to:

$$\text{Lead time at site } l = \frac{\sqrt{r_l^2 + d_{hypo}^2}}{V_s} - \frac{\sqrt{r_{trigger}^2 + d_{hypo}^2}}{V_p} - \delta_t \quad (19)$$

r_l is the site epicentral distance, d_{hypo} is the depth of the earthquake, V_s is the average S-wave velocity, $r_{trigger}$ is the epicentral distance to the furthest triggered station within the radius of interest, V_p is the average P-wave velocity, and δ_t is a delay time that accounts for data telemetry and the time window of information required by EEW algorithms to compute source parameter estimates. $V_p = 6$ km/s and $V_p/V_s = 1.73$ are assumed, according to the 1-D P-wave model and the velocity ratio used in Lin et al. (2010), respectively. $d_{hypo} = 19$ km, that is, the true depth of the 1989 Loma Prieta event. δ_t is taken as 4 s, in line with

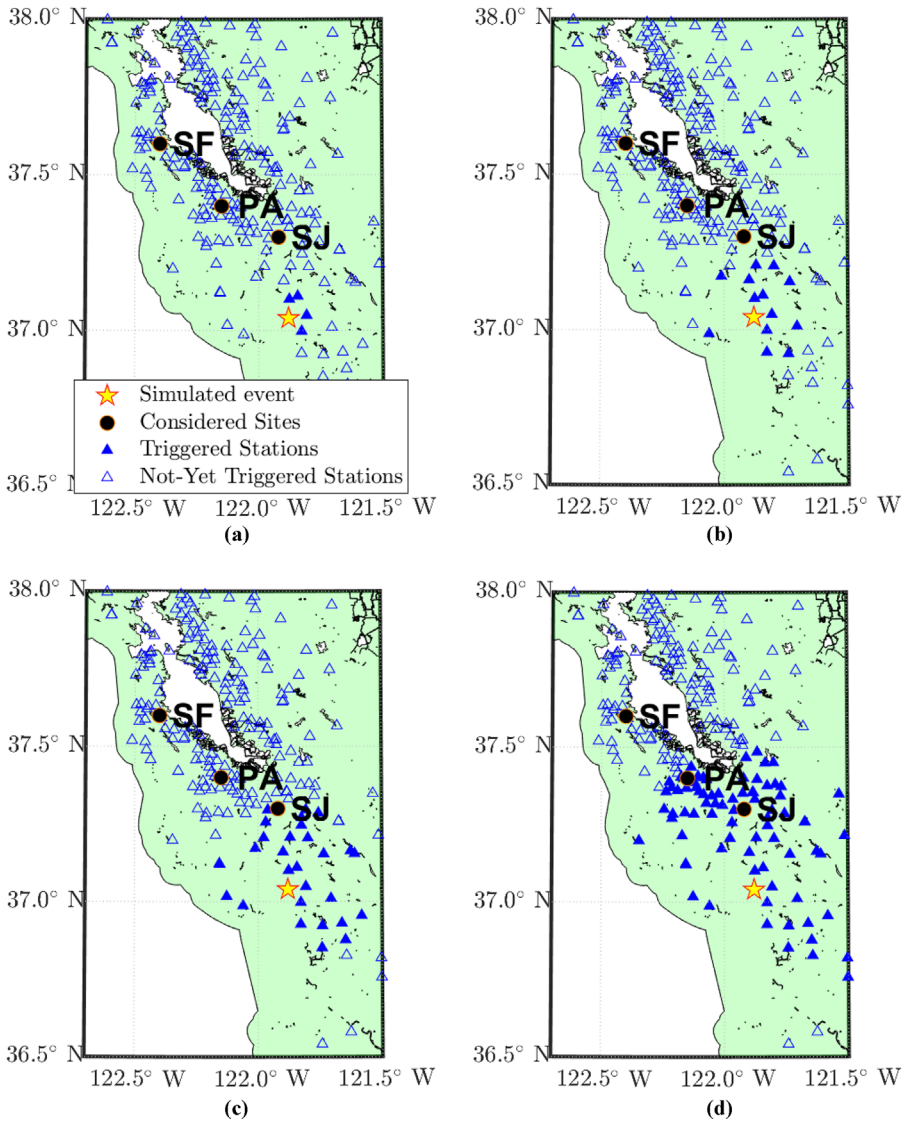

FIGURE 3 Maps displaying the simulated event for the sites considered in Section 3.3, when the incoming P-waves have triggered (a) 4, (b) 13, (c) 29, and (d) 81 stations

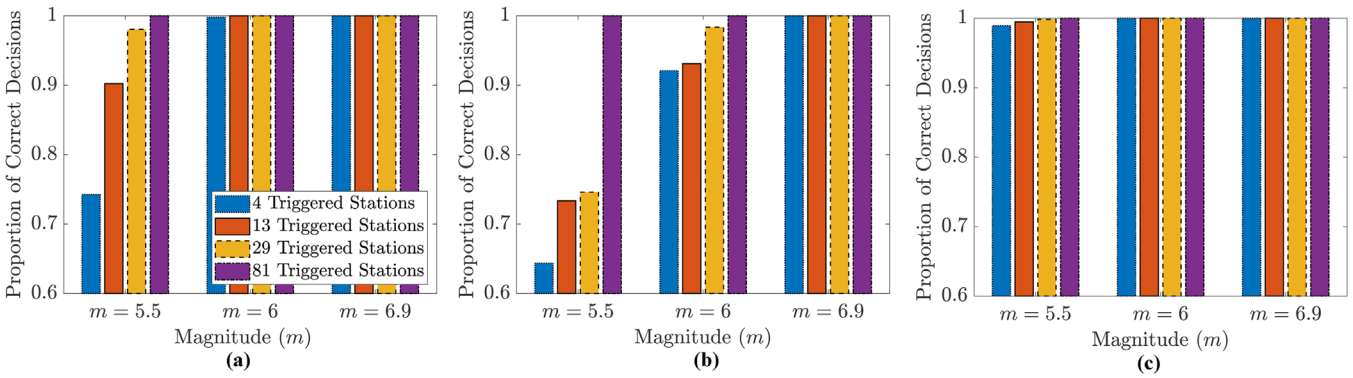

FIGURE 4 Average proportion of the four sets of $\{w_j\}$ considered for which a correct decision is predicted by the Section 3.3 algorithm at the (a) PA site, (b) SF site, and (c) SJ site, as a function of the three simulated events examined and computed using data from different numbers of triggered stations

TABLE 4 Available lead times at examined sites, for simulated earthquakes at the location of the 1989 Loma Prieta event and different radii of triggered stations. Also shown are possible risk-mitigation actions that can be taken in the corresponding warning time, which are adapted from previous work (Goltz, 2002; Iervolino, Galasso et al., 2007; Iervolino, 2011; Oliveira et al., 2015; Porter, 2016; Gobbato et al., 2017)

Triggered station radius	Site	Lead time (s)	Possible actions
10 km	PA	6.9	Performing "drop, cover, and hold on"; Stopping and opening elevators at the nearest floor; Shutting off gas; Shutting down school lab equipment; Evacuating building ground floors.
	SF	15.4	Finding a safe place in an adjacent room; Shutting down industrial equipment; Controlling production lines; Directing traffic away from underpasses; Stopping surgical procedures; Removing vehicles from garages.
	SJ	2.4	Finding a safe place a few steps away; Switching traffic lights to red; Switching on semiactive control systems for structures.
20 km	PA	5.9	Performing "drop, cover, and hold on"; Stopping and opening elevators at the nearest floor; Shutting off gas; Shutting down school lab equipment; Evacuating building ground floors.
	SF	14.4	Finding a safe place in the same room; Shutting down industrial equipment; Controlling production lines; Directing traffic away from underpasses; Stopping surgical procedures; Removing vehicles from garages.
	SJ	1.4	Finding a safe place a few steps away; Switching traffic lights to red; Switching on semiactive control systems for structures.
30 km	PA	4.6	Finding a safe place a few steps away; Switching traffic lights to red; Switching on semiactive control systems for structures.
	SF	13.1	Finding a safe place in the same room; Shutting down industrial equipment; Controlling production lines; Directing traffic away from underpasses; Stopping surgical procedures; Removing vehicles from garages.
	SJ	0.1	—
50 km	PA	1.6	Finding a safe place a few steps away; Switching traffic lights to red; Switching on semiactive control systems for structures.
	SF	10.1	Finding a safe place in the same room; Shutting down industrial equipment; Controlling production lines; Directing traffic away from underpasses; Stopping surgical procedures; Removing vehicles from garages.
	SJ	−2.9	—

previous studies involving the ElarmS algorithm (Kuyuk & Allen, 2013). Table 4 displays available lead times at each site for each triggered station radius, along with potential risk-mitigation actions they enable (for context).

It can be seen in Figure 4 that the accuracy of the predicted optimal action based on precomputed EEW parameters can depend on the magnitude of the incoming earthquake. For example, in the case of SF and a triggered station radius of 10 km, the correct action (i.e., A_1) is predicted for all weighting cases across all 2000 sets of simulated EEW parameter values for $m = 6.9$, but many sets of simulated EEW parameter values incorrectly predict this action for $m = 5.5$. This may be explained by the fact that the true optimal action at SF is constant for all magnitudes close to $m = 6.9$ (and therefore for all $\mathbf{d}$ likely to be observed for this event), whereas the true optimal action switches from $\overline{A}$ to A_1 at magnitudes close to $m = 5.5$ for all weighting cases. Second, as expected, the accuracy of the system increases as more stations are triggered and estimates of the magnitude stabilize. For the specific events and sites examined here, this means that the average accuracy of predicted optimal decisions improves from 79% when four stations are triggered to 100% when 81 stations are triggered. Finally, it is important to note that high accuracy is achieved sufficiently quickly for risk-mitigation actions to be implemented at each examined site if an EEW alarm is triggered. Greater than 99% average accuracy is achieved when 2.4 s of warning time are still available at the nearest site (SJ; 10 km triggered station radius) and when 4.6 s are still available at the middle site (PA; 30 km triggered station radius), which would both enable a safe place to be found a few steps away (see Table 4). Predicted optimal decisions are 100% accurate at the SF site when 10.1 s of warning time are still available (50 km triggered station radius), allowing a safe place to be found in the same room (from Table 4). These lead times justify the case-study assumptions made

about consequences mitigated (i.e., noncollapse casualties and laptop breakages avoided) when an EEW alert is triggered. Potential warning times could be used as additional inputs to the methodology to ensure that data provided on consequences mitigated for given actions is reasonable, using information from the final column of Table 4; however further discussion on this topic is left to future work.

4 | CONCLUSIONS

This study has developed a novel methodology for risk-informed EEW that uniquely combines multi-criteria decisional and earthquake-engineering-related tools, for informed stakeholder-driven decision making. In particular, the proposed methodology can be used to select the optimal risk-mitigation action for current seismic hazard conditions, accounting for stakeholder priorities toward multiple types of uncertain consequences that do not need to be measured in monetary terms.

The proposed methodology was applied to EEW in a hypothetical Californian school, considering the traditional performance metrics (consequences) assessed in PBEE and a range of stakeholder preferences toward them. This application clearly demonstrated that the optimal risk-management action for a given level of impending shaking can depend on stakeholder priorities. For example (based on completely assumptive data), it was found that the school's EEW system would trigger at a site in Palo Alto approximately once every 10 years if stakeholders placed higher importance on limiting casualties, whereas it would only trigger approximately half as frequently if stakeholders prioritized the mitigation of downtime. This finding emphasizes the importance of considering end-user preferences in short-term earthquake risk management, which should be accounted for in future installations of EEW.

Furthermore, it was shown that the methodology can be used to make decisions as a function of (1) magnitude–distance pairs, as well as (2) seismic station/early signal data that act as input to EEW algorithms for estimating source parameters. Decision making based on (2) is particularly useful as it is more representative of realistic scenarios (where information on the incoming event is uncertain) and the required EEW algorithm data can be precomputed offline ahead of the event for efficient real-time risk management. For three different sites of the hypothetical school, three scenario events and one source location, it was found that the proportion of correct EEW decisions based on (2) increases with the density of stations triggered (as expected) and high accuracy is reached sufficiently quickly for risk-mitigation actions to be implemented, underlining the credibility of the proposed methodology. Future work will explicitly treat potential warning times as an input of the methodology, to guide the selection of appropriate and feasible case-specific risk-management actions in further applications.

The results of this study represent a significant advancement over state-of-the art risk-based decision-making methods for EEW that mainly rely on cost–benefit analyses. The developed algorithm could be packaged as a software plug-in to existing operational EEW platforms, transforming these systems into powerful end-user-driven tools that effectively promote and prioritize seismic resilience.

ACKNOWLEDGMENTS

The authors thank the editor and seven anonymous reviewers for constructive feedback that significantly improved this manuscript. This research is funded by the European Union's Horizon 2020 research and innovation programme, specifically grant agreement number 821046: TURNkey "*Towards more Earthquake-resilient Urban Societies through a Multi-sensor-based Information System enabling Earthquake Forecasting, Early Warning and Rapid Response actions*." An academic license of the SP3 software (www.hbrisk.com) was used to perform FEMA P-58 analyses.

AUTHOR CONTRIBUTIONS

Both authors helped to conceive and design the research. G.C. drafted the written content of the manuscript, which C.G. also reviewed. G.C. performed the calculations. Both authors developed the figures.

CONFLICT OF INTEREST

There are no conflicts of interest associated with this research.

REFERENCES

Allen, R. M., & Melgar, D. (2019). Earthquake early warning: Advances, scientific challenges, and societal needs. *Annual Review of Earth and Planetary Sciences*, *47*, 361–388.Retrieved from https://doi.org/10.1146/annurev-earth-053018

Baker, J. W., & Cornell, C. A. (2005). A vector-valued ground motion intensity measure consisting of spectral acceleration and epsilon. *Earthquake Engineering and Structural Dynamics*, *34*(10), 1193–1217.

Baker, J. W., & Cornell, C. A. (2006). Spectral shape, epsilon and record selection. *Earthquake Engineering and Structural Dynamics*, *35*(9), 1077–1095.

Baker, J. W., & Jayaram, N. (2008). Correlation of spectral acceleration values from NGA ground motion models. *Earthquake Spectra*, *24*(1), 299–317.

Boore, D. M., Stewart, J. P., Seyhan, E., & Atkinson, G. M. (2014). *NGA-West 2 Equations for predicting PGA, PGV, and 5%-damped PSA for shallow crustal earthquakes* (Tech. Rep.). Retrieved from http://peer.berkeley.edu

Bozza, A., Asprone, D., Parisi, F., & Manfredi, G. (2017). Alternative resilience indices for city ecosystems subjected to natural hazards. *Computer-Aided Civil and Infrastructure Engineering*, *32*(7), 527–545.

Brown, H. M., Allen, R. M., Hellweg, M., Khainovski, O., Neuhauser, D., & Souf, A. (2011). Development of the ElarmS methodology for earthquake early warning: Realtime application in California and offline testing in Japan. *Soil Dynamics and Earthquake Engineering*, *31*(2), 188–200.

Burton, H. V., Miles, S. B., & Kang, H. (2018). Integrating performance-based engineering and urban simulation to model post-earthquake housing recovery. *Earthquake Spectra*, *34*(4), 1763–1785.

Caterino, N., Iervolino, I., Manfredi, G., & Cosenza, E. (2008). Multicriteria decision making for seismic retrofitting of RC structures. *Journal of Earthquake Engineering*, *12*(4), 555–583.

Caterino, N., Iervolino, I., Manfredi, G., & Cosenza, E. (2009). Comparative analysis of multi-criteria decision-making methods for seismic structural retrofitting. *Computer-Aided Civil and Infrastructure Engineering*, *24*(6), 432–445.

Cauzzi, C., Behr, Y., Le Guenan, T., Douglas, J., Auclair, S., Woessner, J., … Wiemer, S. (2016). Earthquake early warning and operational earthquake forecasting as real-time hazard information to mitigate seismic risk at nuclear facilities. *Bulletin of Earthquake Engineering*, *14*(9), 2495–2512.

Chung, A. I., Meier, M.-A., Andrews, J., Böse, M., Crowell, B. W., McGuire, J. J., & Smith, D. E. (2020). ShakeAlert earthquake early warning system performance during the 2019 Ridgecrest earthquake sequence. *Bulletin of the Seismological Society of America*, *110*(4), 1904–1923.

Cremen, G., & Baker, J. (2018). Quantifying the benefits of building instruments to FEMA P-58 rapid post-earthquake damage and loss predictions. *Engineering Structures*, *176*, 243–253.

Cremen, G., & Galasso, C. (2020). Earthquake early warning: Recent advances and perspectives. *Earth-Science Reviews*, 103184.

Cremen, G., Galasso, C., & Zuccolo, E. (2021). Could earthquake early warning be effective across Europe? *Nature Communications*, (in review).

Cuéllar, A., Suárez, G., & Espinosa-Aranda, J. M. (2017). Performance evaluation of the earthquake detection and classification algorithm 2 (tS-tP) of the seismic alert system of Mexico (SASMEX). *Bulletin of the Seismological Society of America*, *107*(3), 1451–1463.

Dyer, J. S. (2005). MAUT—multiattribute utility theory. In *Multiple criteria decision analysis: State of the art surveys* (pp. 265–292). New York: Springer.

FEMA. (2010). *FEMA P-424: Design guide for improving school safety in earthquakes, floods, and high winds* (Tech. Rep.). Washington, DC: Author.

FEMA. (2013). *Hazus-MH 2.1: Technical manual*. Washington, DC: Author.

FEMA. (2018). *Seismic performance assessment of buildings, Volume 1—Methodology* (Tech. Rep.). Washington, DC: Author.

Gasparini, P., Manfredi, G., & Zschau, J. (2011). Earthquake early warning as a tool for improving society's resilience and crisis response. *Soil Dynamics and Earthquake Engineering*, *31*(2), 267–270.

Gentile, R., & Galasso, C. (in press). Simplified seismic loss assessment for optimal structural retrofit of RC buildings. *Earthquake Spectra*.

Gobbato, M., Shome, N., & Woo, G. (2017). *The cost-effectiveness of a public Californian earthquake early warning system*. 16th World Conference on Earthquake Engineering, Santiago.

Goda, K. (2015). Seismic risk management of insurance portfolio using catastrophe bonds. *Computer-Aided Civil and Infrastructure Engineering*, *30*(7), 570–582.

Goda, K., & Hong, H. P. (2006). Optimal seismic design considering risk attitude, societal tolerable risk level, and life quality criterion. *Journal of Structural Engineering*, *132*(12), 2007–2035.

Goltz, J. D. (2002). *Introducing earthquake early warning in California—A summary of social science and public policy issues* (Tech. Rep.). Pasadena, CA: Governor's Office of Emergency Services.

Grasso, V. F. (2005). *Seismic early warning systems: Procedure for automated decision making* (PhD thesis). Università degli Studi di Napoli Federico II.

Grasso, V. F., Beck, J. L., & Manfredi, G. (2007). Automated decision procedure for earthquake early warning. *Engineering Structures*, *29*(12), 3455–3463.

Haselton, C. B., & Deierlein, G. G. (2007). *Assessing seismic collapse safety of modern reinforced concrete moment-frame buildings* (Tech. Rep.).

Hsu, T. Y., Wu, R. T., & Chang, K. C. (2016). Two novel approaches to reduce false alarm due to non-earthquake events for on-site earthquake early warning system. *Computer-Aided Civil and Infrastructure Engineering*, *31*(7), 535–549.

Iervolino, I. (2011). Performance-based earthquake early warning. *Soil Dynamics and Earthquake Engineering*, *31*(2), 209–222.

Iervolino, I., Galasso, C., & Manfredi, G. (2007). *Information-dependent lead-time maps for earthquake early warning in the Campania region*. 14th World Conference on Earthquake Engineering, Beijing. Retrieved from http://www.rissclab.unina.it

Iervolino, I., Giorgio, M., Galasso, C., & Manfredi, G. (2009). Uncertainty in early warning predictions of engineering ground motion parameters: What really matters? *Geophysical Research Letters*, *36*(4), L00B06.

Iervolino, I., Giorgio, M., & Manfredi, G. (2007). Expected loss-based alarm threshold set for earthquake early warning systems. *Earthquake Engineering and Structural Dynamics*, *36*(9), 1151–1168.

Krawinkler, H., Zareian, F., Medina, R. A., & Ibarra, L. F. (2006). Decision support for conceptual performance-based design. *Earthquake Engineering and Structural Dynamics*, *35*(1), 115–133.

Kuyuk, H. S., & Allen, R. M. (2013). Optimal seismic network density for earthquake early warning: A case study from California. *Seismological Research Letters*, *84*(6), 946–954.

Le Guenan, T., Smai, F., Loschetter, A., Auclair, S., Monfort, D., Taillefer, N., & Douglas, J. (2016). Accounting for end-user preferences in earthquake early warning systems. *Bulletin of Earthquake Engineering*, *14*(1), 297–319.

Lin, G., Thurber, C. H., Zhang, H., Hauksson, E., Shearer, P. M., Waldhauser, F., … Hardebeck, J. (2010). A California statewide three-dimensional seismic velocity model from both absolute and differential times. *Bulletin of the Seismological Society of America*, *100*(1), 225–240.

Maddaloni, G., Caterino, N., & Occhiuzzi, A. (2011). Semi-active control of the benchmark highway bridge based on seismic early warning systems. *Bulletin of Earthquake Engineering*, *9*(5), 1703–1715.

May, P. J. (2004). Making choices about earthquake performance. *Natural Hazards Review*, *5*(2), 64–70.

McBride, S., Bostrom, A., Sutton, J., de Groot, R. M., Baltay, A. S., Terbush, B., … Vinci, M. (2020). Developing post-alert messaging for ShakeAlert, the earthquake early warning system for the West Coast of the United States of America. *International Journal of Disaster Risk Reduction*, *50*, 101713.

Meier, M. A., Ross, Z. E., Ramachandran, A., Balakrishna, A., Nair, S., Kundzicz, P., … Yue, Y. (2019). Reliable real-time seismic signal/noise discrimination with machine learning. *Journal of Geophysical Research: Solid Earth*, *124*(1), 788–800.

Miranda, E. (1999). *Approximate seismic lateral deformation demands in multistory buildings* (Tech. Rep.).

Moehle, J., & Deierlein, G. G. (2004). *A framework methodology for performance-based earthquake engineering*. 13th World Conference on Earthquake Engineering, Vancouver.

Mosalam, K. M., Alibrandi, U., Lee, H., & Armengou, J. (2018). Performance-based engineering and multi-criteria decision analysis for sustainable and resilient building design. *Structural Safety*, *74*, 1–13.

NCEDC. (2014). Northern California Earthquake Data Center Dataset. UC Berkeley Seismological Laboratory. Dataset. https://doi.org/10.7932/NCED

Oliveira, C. S., Mota de Sá, F., Lopes, M., Ferreira, M. A., & Pais, I. (2015). Early warning systems: Feasibility and end-users' point of view. *Pure and Applied Geophysics*, *172*(9), 2353–2370.

O'Reilly, G. J., Perrone, D., Fox, M., Monteiro, R., & Filiatrault, A. (2018). Seismic assessment and loss estimation of existing school buildings in Italy. *Engineering Structures*, *168*, 142–162.

Ouyang, M., & Fang, Y. (2017). A mathematical framework to optimize critical infrastructure resilience against intentional attacks. *Computer-Aided Civil and Infrastructure Engineering*, *32*(11), 909–929.

Panakkat, A., & Adeli, H. (2008). Recent efforts in earthquake prediction (1990–2007). *Natural Hazards Review*, *9*(2), 70–80.

Petersen, M. D., Moschetti, M. P., Powers, P. M., Mueller, C. S., Haller, K. M., Frankel, A. D., … Olsen, A. H. (2014). *Documentation for the 2014 update of the United States National Seismic Hazard Maps* (Tech. Rep.). U.S. Geological Survey.

Petersen, M. D., Shumway, A. M., Powers, P. M., Mueller, C. S., Moschetti, M. P., Frankel, A. D., … Zeng, Y. (2020). The 2018 update of the US National Seismic Hazard Model: Overview of model and implications. *Earthquake Spectra*, *36*(1), 5–41.

Porter, K. A. (2016). *How many injuries can be avoided through earthquake early warning and drop, cover, and hold on?* (Tech. Rep.). Boulder, Co: Structural Engineering and Structural Mechanics Program, Department of Civil Environmental and Architectural Engineering, University of Colorado.

Porter, K. A., Scawthorn, C. R., & Beck, J. L. (2006). Cost-effectiveness of stronger woodframe buildings. *Earthquake Spectra*, *22*(1), 239–266.

Rafiei, M. H., & Adeli, H. (2017). NEEWS: A novel earthquake early warning model using neural dynamic classification and neural dynamic optimization. *Soil Dynamics and Earthquake Engineering*, *100*, 417–427.

Saadat, S., Camp, C. V., & Pezeshk, S. (2014). Seismic performance-based design optimization considering direct economic loss and direct social loss. *Engineering Structures*, *76*, 193–201.

Saaty, T. L. (1980). *The analytic hierarchy process: Planning, priority setting, resource allocation*. New York: McGraw-Hill International Book Co.

Salzano, E., Garcia Agreda, A., Di Carluccio, A., & Fabbrocino, G. (2009). Risk assessment and early warning systems for industrial facilities in seismic zones. *Reliability Engineering and System Safety*, *94*(10), 1577–1584.

Satriano, C., Elia, L., Martino, C., Lancieri, M., Zollo, A., & Iannaccone, G. (2011). PRESTo, the earthquake early warning system for Southern Italy: Concepts, capabilities and future perspectives. *Soil Dynamics and Earthquake Engineering*, *31*(2), 137–153.

Satriano, C., Wu, Y. M., Zollo, A., & Kanamori, H. (2011). Earthquake early warning: Concepts, methods and physical grounds. *Soil Dynamics and Earthquake Engineering*, *31*(2), 106–118.

Sharma, N., Tabandeh, A., & Gardoni, P. (2020). Regional resilience analysis: A multiscale approach to optimize the resilience of interdependent infrastructure. *Computer-Aided Civil and Infrastructure Engineering*, *35*(12), 1315–1330.

Stewart, M., & Melchers, R. E. (1997). *Probabilistic risk assessment of engineering systems*. Netherlands: Springer.

Tesfamariam, S., Sadiq, R., & Najjaran, H. (2010). Decision making under uncertainty—An example for seismic risk management. *Risk Analysis*, *30*(1), 78–94.

The National Institute of Building Sciences. (2010). *Concrete model building subtypes—Recommended for use in collecting inventory data* (Tech. Rep.). Gaithersburg, MD: The National Institute of Standards and Technology.

Thompson, E. M., & Worden, C. B. (2018). Estimating rupture distances without a rupture. *Bulletin of the Seismological Society of America*, *108*(1), 371–379.

Viscusi, W. K., & Masterman, C. J. (2017). Income elasticities and global values of a statistical life. *Journal of Benefit-Cost Analysis*, *8*(2), 226–250.

Wang, J. P., Wu, Y. M., Lin, T. L., & Brant, L. (2012). The uncertainties of a Pd3-PGV onsite earthquake early warning system. *Soil Dynamics and Earthquake Engineering*, *36*, 32–37.

Wu, S., Beck, J. L., & Heaton, T. H. (2013). ePAD: Earthquake probability-based automated decision-making framework for earthquake early warning. *Computer-Aided Civil and Infrastructure Engineering*, *28*(10), 737–752.

Wu, S., Cheng, M. H., Beck, J. L., & Heaton, T. H. (2016). An engineering application of earthquake early warning: EPAD-based decision framework for elevator control. *Journal of Structural Engineering (United States)*, *142*(1).04015092

Wurman, G., Allen, R. M., & Lombard, P. (2007). Toward earthquake early warning in northern California. *Journal of Geophysical Research: Solid Earth*, *112*.B08311

Xiong, C., Huang, J., & Lu, X. (2020). Framework for city-scale building seismic resilience simulation and repair scheduling with labor constraints driven by time–history analysis. *Computer-Aided Civil and Infrastructure Engineering*, *35*(4), 322–341.

Yong, A., Thompson, E. M., Wald, D. J., Knudsen, K. L., Odum, J. K., Stephenson, W. J., & Haefner, S. (2015). *Compilation of V S30 data for the United States* (Tech. Rep. US Geological Survey.

Yoon, & Hwang (1995). Sage Publications Thousand Oaks, London, New Dehli

Yoon, K. P., & Hwang, C.-L. (1995). *Multiple attribute decision making: An introduction*. Thousand Oaks, CA, London, New Dehli: Sage.

Zhang, J., Hegde, G. G., Shang, J., & Qi, X. (2016). Evaluating emergency response solutions for sustainable community development by using fuzzy multi-criteria group decision making approaches: IVDHF-TOPSIS and IVDHF-VIKOR. *Sustainability*, *8*(4), 291.

Zhou, L., Wu, X., Xu, Z., & Fujita, H. (2018). Emergency decision making for natural disasters: An overview. *International Journal of Disaster Risk Reduction*, *27*, 567–576.

How to cite this article: Cremen G, Galasso C. A decision-making methodology for risk-informed earthquake early warning. *Comput Aided Civ Inf*. 2021;1–15. https://doi.org/10.1111/mice.12670

APPENDIX A: ALGORITHM

Algorithm 1 contains the decision-making algorithm proposed in this paper. All variables are as defined in Section 2.

ALGORITHM 1 Identifying the Optimal EEW Decision

Step 1: Mod_PBEE

1.1: Determine $f(\mathbf{im}|\mathbf{d})$, based on the relevant EEW algorithm.

1.2: Use the result of Step 1.1 and required structural modeling information (see Appendix C) to generate $E^{\overline{A}}(C_j^{\overline{A}}|\mathbf{d})$, based on the PBEEW framework provided in Equation (1).

1.3: Calculate $p(FA|\mathbf{d})$ according to Equation (4).

1.4: Use the results of Steps 1.2 and 1.3, as well as stakeholder-reported values of c_{ij}^{FA} and $\alpha_{ij}(\mathbf{d})$, to calculate $E^{A_i}(C_j^{A_i}|\mathbf{d}) = p(FA|\mathbf{d})c_{ij}^{FA} + \alpha_{ij}(\mathbf{d})E^{\bar{A}}(C_j^{\bar{A}}|\mathbf{d})$.

1.5: Repeat Step 1.4 for all N_a actions and N_c consequence criteria, to develop the consequence matrix.

Step 2: Mod_MCDM

2.1: Use the results of Step 1.5 to generate r_{A_i,C_j} according to Equation (6).

2.2: Use stakeholder-reported values of w_j to calculate $r_{A_i,C_j}w_j$.

2.3: Repeat Steps 2.1 and 2.2 for all N_a actions and $\overline{A}$, and N_c consequence criteria, to develop the decision matrix.

Step 3: Mod_Decision

3.1: Use the results of Step 2.3 to calculate $v_j^+ = \min_j(r_{A_1,C_j}w_j, \dots, r_{A_{N_a},C_j}w_j, r_{\overline{A},C_j}w_j)$ and $v_j^- = \max_j(r_{A_1,C_j}w_j, \dots, r_{A_{N_a},C_j}w_j, r_{\overline{A},C_j}w_j)$.

3.2: Use the results of Steps 2.3 and 3.1, and Equations (7)–(9), to determine the optimal action.

APPENDIX B: DERIVING EQUATION (17)

Using Equation (14) and accounting for the assumptions that P_d measurements are lognormally distributed as well as independent, the likelihood function for these measurements across N_s stations can be expressed as:

$$f\left(P_{d_1}, P_{d_2}, \dots, P_{d_{N_s}}|m\right) = \left(\frac{1}{\sqrt{2\pi}\sigma_{\ln(P_d)}}\right)^{N_s}\left(\prod_{k=1}^{N_s}\frac{1}{P_{d_k}}\right) e^{-\frac{1}{2}\left(\frac{\sum_{k=1}^{N_s}\left(\ln\left(P_{d_k}\right)\right)^2}{\sigma_{\ln P_d}^2}\right)} e^{\left(\frac{\sum_{k=1}^{N_s}\left(2\ln(P_{d_k})\mu_{\ln(P_{d_k})}-\mu_{\ln(P_{d_k})}^2\right)}{2\sigma_{\ln P_d}^2}\right)} \tag{B.1}$$

By (1) substituting Equations (B.1) and (12) into Equation (11); and (2) canceling the $\left(\frac{1}{\sqrt{2\pi}\sigma_{\ln(P_d)}}\right)^{N_s}$, $\left(\prod_{k=1}^{N_s}\frac{1}{P_{d_k}}\right)e^{-\frac{1}{2}\left(\frac{\sum_{k=1}^{N_s}\left(\ln\left(P_{d_k}\right)\right)^2}{\sigma_{\ln P_d}^2}\right)}$, and $\left(\frac{\beta}{e^{-\beta M_{min}}-e^{-\beta M_{max}}}\right)$ terms that are common to the numerator and the denominator, the expression for $f(m|\mathbf{d})$ becomes:

$$f(m|\mathbf{d}) = \frac{e^{\frac{\sum_{k=1}^{N_s}\left(2\ln(P_{d_k})\mu_{\ln(P_{d_k})}-\mu_{\ln(P_{d_k})}^2\right)}{2\sigma_{\ln P_d}^2}} e^{-\beta m}}{\int_{M_{min}}^{M_{max}} e^{\frac{\sum_{k=1}^{N_s}\left(2\ln(P_{d_k})\mu_{\ln(P_{d_k})}-\mu_{\ln(P_{d_k})}^2\right)}{2\sigma_{\ln P_d}^2}} e^{-\beta m}\, dm} \tag{B.2}$$

Substituting Equation (15) for $\mu_{\ln(P_{d_k})}$ reduces Equation (B.2) to (17) for:

$$\begin{aligned} x(\mathbf{d}) = x_1 &\left[2md_1 - 2\left(x_2d_3 + x_3d_1\right) - N_sx_1m^2\right) \\ &+ 2x_1m\left(x_2d_2 + N_sx_3\right) \\ &- \left(x_1\left(x_2^2d_4 + 2x_2x_3d_2 + N_sx_3^2\right)\right] \end{aligned} \tag{B.3}$$

where $d_3 = \sum_{k=1}^{N_s}\ln(P_{d_k})\log_{10}(r_k)$, $d_4 = \sum_{k=1}^{N_s}\log_{10}(r_k^2)$, and all other variables are as defined previously. Finally, canceling nonmagnitude-dependent terms (since they are common to both the numerator and the denominator of Equation 17) simplifies Equation (B.3) to (18).

APPENDIX C: STRUCTURAL MODELING DETAILS

Structural modeling details are provided in Table C.1.

TABLE C.1 Structural modeling details of the hypothetical school, including FEMA P-58 parameters. Note that the FEMA P-58 analyses were run using the SP3 software (https://www.hbrisk.com/)

Parameter	Value	Additional notes/Justification
Year of construction	2003	
Occupancy	Elementary school	
Number of stories	2	Corresponds with typical characteristics of suburban U.S. schools (FEMA, 2010; The National Institute of Building Sciences, 2010)
Lateral system	Reinforced concrete space moment frame	
Length in direction 1 (m)	26	Corresponds with plan layout of precast concrete school modeled in O'Reilly et al. (2018)
Length in direction 2 (m)	42	
Story height (m)	4	
Fundamental period (T_1) (s)	0.4	FEMA (2013) assumed value for building
Yield base shear coefficient (V_y)	0.1663 g	SP3 default input values to the FEMA P-58 simplified analysis procedure (detailed in Section 5.3 of FEMA (2018)) for building. a and α are used in the lateral displacement equations of Miranda (1999), to compute the Δ_i variable of the simplified methodology according to eqs. 5–10 of FEMA (2018).
Yield story drift ratio (Δ_y)	0.0075	
First mode mass ratio	1	
a	0.01	
α	12.5	
Soil site class	D	Corresponds with assumed $Vs30$ values at each site
Collapse capacity	Lognormally distributed with 10% probability of collapse for hazard level with 2% probability of exceedance in 50 years and dispersion = 0.6	Assumed model, in line with previous studies for buildings of similar age and identical lateral system (e.g., Haselton & Deierlein, 2007); FEMA P-58 default value for collapse dispersion. Hazard levels are computed at each site using the 2018 US National Seismic Hazard Model (Petersen et al., 2020)
FEMA P-58 structural components	ACI 318 concrete SMF (B1041.002a & B1041.002b)	SP3 default components for building, except UD. UD has user-defined cost and repair time
FEMA P-58 nonstructural components	Wall partition, metal stud (C1011.001a); HVAC ducting (D3041.011c); curtain walls (B2022.002); suspended ceiling (C3032.003a, C3032.003b, C3032.003c, & C3032.003d); independent pendant lighting (C3034.002); concrete stairs with seismic joints (C2011.011a); desktop electronics including computers, monitors, stereos, etc. on a slip resistant surface (UD)	consequence distributions, which are set as follows: cost is normally distributed with mean = \$500 and standard deviation = 0.05; repair time is normally distributed with mean = 0.1 day and standard deviation = 0.05
FEMA P-58 component quantities	10 UD per floor; all other quantities are P-58 median values for building layout	
Building population model	FEMA P-58 default model for occupancy	
Building replacement cost (\$ per sq. ft.)	270	SP3 default value for building
Building replacement time (days per story)	169	SP3 default value for building
Building repair time type	Serial	